Simulation Studies of Single-Event Effects in β-Ga_2O_3 MOSFETs

Animesh Datta and Uttam Singisetti, *Senior Member, IEEE*

***Abstract*—In this article, we investigate the single-event effects (SEEs) leading to single-event burnout (SEB) in β-Ga_2O_3 MOSFETs. Using Silvaco TCAD, 2-D simulations were performed to understand the mechanism behind the SEB mechanism in lateral Ga_2O_3 MOSFETs. The high electric fields in the channel played a critical role leading to high impact generation rates and eventual SEB. To reduce the electric field in the channel, radiation-hardened designs are then proposed with rounded gates and the use of a combination of high-permittivity (k) dielectric with SiO_2. With HfO_2–SiO_2 dielectric combination, the SEB threshold of 550 V at LET = 10 MeV/mg/cm^2 is seen. However, to operate under extreme radiation conditions, a combination of very high-k dielectric material $BaTiO_3$ with SiO_2 is proposed. Using the radiation-hardened design, SEB thresholds up to 1000 V for LET = 75 MeV/mg/cm^2 could be achieved which is higher than the state-of-the-art technology. The energy dissipated during the ion strike event is also calculated and it is observed that it is lower than that of SiC MOSFETs. However the energy dissipation value is not directly correlated with an SEB threshold condition.**

***Index Terms*—Electric field, Ga_2O_3 MOSFETs, radiation, single-event burnout (SEB), single-event effects (SEEs).**

I. Introduction

RADIATION damages are a common reliability issue for power electronic devices used for space applications. Harsh radiation conditions in space can cause reliability problems such as temporary loss of data, circuit degradation, and loss of functional operation to destruction of the semiconductor device [1], [2], [3]. Radiation effects are typically classified into cumulative effects such as total ionizing dose (TID) effects, or single-event effects (SEEs) leading to single-event burnout (SEB). These effects lead to defect generation, device degradation, and device failures. Previous studies have suggested that SEEs are more dominant than cumulative effects in wide bandgap materials [4], [5], [6], [7]. There have been significant experimental and simulation studies of radiation effects especially SEEs in SiC [8], [9], [10], [11], [12], [13], [14], [15] and GaN [16], [17], [18], [19] devices. Recent reports have also explored SEE in ultrawide bandgap AlGaN HEMTs [20] and MISFETs [21] to design radiation-hardened devices.

Manuscript received 5 September 2023; revised 25 October 2023; accepted 30 October 2023. Date of publication 14 November 2023; date of current version 2 January 2024. This work was supported in part by the Air Force Office of Scientific Research (AFOSR) under Award FA9550-18-1-0479 (Program Manager: Ali Sayir) and in part by NSF under Award ECCS 2019749 and Award ECCS 2231026. The review of this article was arranged by Editor M. Meneghini. *(Corresponding author: Uttam Singisetti.)*

The authors are with the Electrical Engineering Department, University at Buffalo, Buffalo, NY 14260 USA (e-mail: uttamsin@buffalo.edu).

Color versions of one or more figures in this article are available at https://doi.org/10.1109/TED.2023.3330132.

Digital Object Identifier 10.1109/TED.2023.3330132

β-Ga_2O_3 with its large band gap of 4.8–4.9 eV and high critical electric field strength of 8 MV/cm [22], [23] has promising potential for power electronics and RF applications. Another advantage of β-Ga_2O_3 is the availability of large-diameter wafers. Common growth techniques such as Czochralski (CZ), float-zone (FZ), edge-defined film fed (EFG), or Bridgman can be used to grow bulk crystals [24], [25], [26]. Recent experimental reports have shown high breakdown voltages (multi-kVs) and high figure of merit in β-Ga_2O_3 lateral MOSFETs [27], [28], [29], [30], [31], [32], [33] and Schottky diodes [34], [35], [36], [37], [38]. Previously there have been studies of neutron damage, X-ray damage, and gamma-ray damage in β-Ga_2O_3 MOSFETs [4], [39], [40], [41], [42] but there has been no extensive study on SEEs in these devices despite it being a favorable ultrawide bandgap semiconductor.

In this work, we investigate the SEEs in β-Ga_2O_3 MOSFETs using 2-D TCAD simulations. Initially, a baseline design of lateral β-Ga_2O_3 MOSFET with SiO_2 dielectric is simulated under various radiation conditions. The SEB threshold of 200 V for LET = 10 MeV/mg/cm^2 for this device is lower than the simulated SEB of AlGaN/GaN channel MISFETs which has a threshold of 430 V at LET = 21 MeV/mg/cm^2 [21]. The physics behind the SEB mechanism is investigated which helps us in proposing radiation-hardened designs. The simulations suggest that the use of a combination of high-k dielectric with SiO_2 is crucial for full device recovery under extreme radiation conditions. Using a conventional HfO_2 dielectric increases the SEB threshold voltage from 220 to 550 V at LET = 10 MeV/mg/cm^2 which is higher than that of GaN channel HEMTs [20]. But this design is still susceptible to SEB at higher linear energy transfers (LETs) and operating biases. Recent reports have suggested the use of a $BaTiO_3$ on β-Ga_2O_3 to achieve high breakdown voltage devices [43]. There have also been reports

of using $BaTiO_3$ on AlGaN to design state-of-the-art breakdown voltage diodes [44] and HEMTs [45]. $BaTiO_3$ has a reported dielectric constant of >100 for thin films. Thus, a design with an extreme high-k dielectric ($BaTiO_3$) in combination with SiO_2 is proposed which shows full recovery for all the radiation conditions. With this design, SEB thresholds of 1000 V at LET = 75 MeV/mg/cm^2 can be achieved which is higher than the state-of-the-art technology.

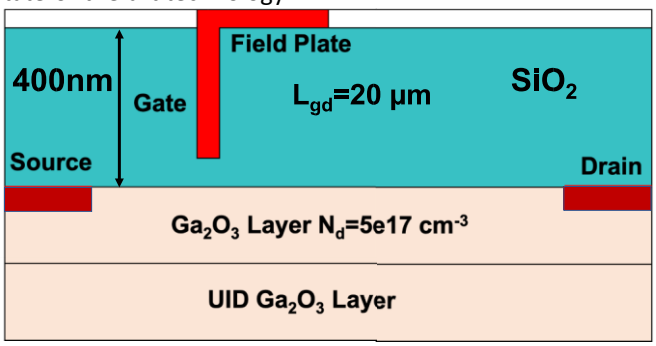

Fig. 1. Device schematic of the simulated baseline lateral MOSFET.

II. Device Structure and Models

Fig. 1 shows the device structure of the baseline Ga_2O_3 MOSFET. The channel layer is 200-nm thick with a doping concentration of 5×10^{17} cm^{-3}. The ohmic layers, used for the drain and source contacts, are 50-nm thick and heavily doped with a concentration of 1×10^{19} cm^{-3}. The gate electrode has a work function of 4.8 eV. Field plate edge termination technique [29], [30] is used to maximize the breakdown voltage of the device. The device was simulated using the 2-D simulator of SILVACO ATLAS. The models used in the simulation include the SRH recombination model, Auger recombination model, impact ionization model, and field-dependent mobility model. According to previous studies from first principle calculations [46], [47] the low field mobility of Ga_2O_3 is taken to be 150 cm^2/V-s for a doping concentration of 5×10^{17} cm^{-3}. The hole mobility in the channel is taken to be 0.1 cm^2/V-s which is quite low due to the weakly interacting O 2p states which create deep acceptors. The impact ionization parameters for β-Ga_2O_3 have been taken from a detailed first principle theoretical study [48]. Fig. 2 shows the output and transfer characteristics of the device. The threshold voltage of the device from Fig. 2 is −20 V.

The breakdown voltage of the device is determined by analyzing the electric field contour plots at specified operating bias. Fig. 3 shows the electric field profile at the breakdown voltage of the device. The device breakdown is determined when the electric field in the channel exceeds the critical breakdown field of SiO_2 and Ga_2O_3. As shown in Fig. 3 at 1500 V, the field in the channel is close to 7 MV/cm and that of SiO_2 is 25 MV/cm which is close to their critical breakdown fields [49]. Thus, the breakdown voltage of the device is estimated to be 1500 V, which is close to the experimentally reported breakdown voltage [29], [30] at comparable gate–drain spacing.

III. Single-Event Effects

SEEs occur when individual energetic particle induces errors or failures in the device or the overall circuit [50], [51]. The incident ionization particle loses energy in the semiconductor through Coulomb interaction with the lattice structure. The energy is transferred to the lattice as an ionization tail of free electron–hole pairs (ehps) leading to transient current. Under heavy ion radiation conditions, a second breakdown mechanism might occur leading to a catastrophic failure of the device known as SEB.

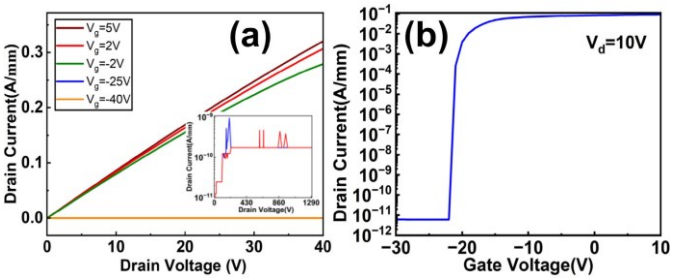

Fig. 2. Simulated (a) output characteristics and (b) transfer characteristics of the MOSFET.

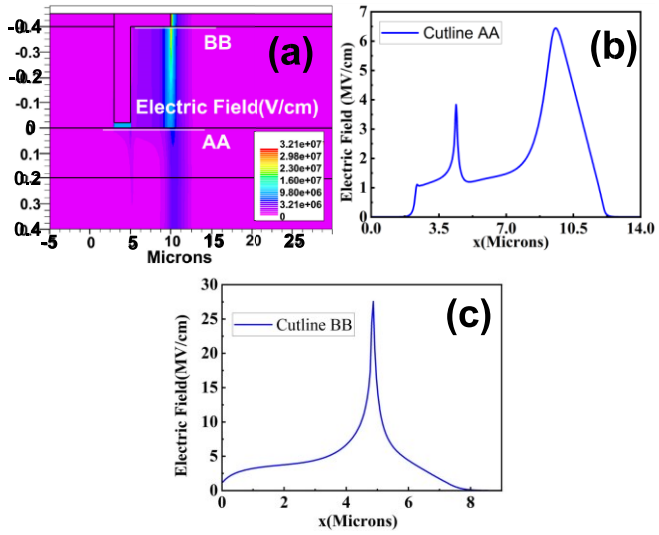

Fig. 3. (a) Silvaco ATLAS simulation of electric field profile at V_{ds} = 1500 V and V_{gs} = −40 V. (b) Field in the Ga_2O_3 channel along cutline AA′. (c) Field in the field plate oxide along cutline BB′.

In radiation studies, a common measure of the loss of energy of the SEU particle, as it suffers collisions in a material, is the LET value, which is given in units of MeV/mg/cm^2. LET is the linear energy transfer of the incident ion which determines the number of ehps created in the material depending on the band structure and the density of the material. The creation energy of an ehps in the semiconductor (ϵ_1) is approximately calculated to be three times the band gap of the material [52]. The number of free carriers released is calculated as [53]

LET(ehp/μm)

$$= \text{LET MeV} \quad \frac{\text{mg}\ 1}{\times\times \text{density}(\text{gm/cm}).(1)\ \text{cm}^2} \quad \epsilon_1^3$$

The amount of ehps created by the ionizing particle can be converted in terms of the linear charge deposited inside the semiconductor in units of pC/μm. Since Ga_2O_3 is a wide bandgap semiconductor, the conversion factor for material comes to be 0.007 pC/μm corresponding to LET = 1 MeV/mg/cm^2. This is quite low compared with 0.1 pC/μm for Si and is comparable to other wide bandgap materials such as GaN and SiC. Thus, the lower charge deposition by the ionizing particle and the highly promising properties Ga_2O_3-based devices might provide better radiation tolerance than other wide bandgap materials.

The SEEs can be simulated using the ATLAS 2-D simulator using the SINGLEEVENTUPSET statement. The radius, length, and time dependence of the charge generation track can be specified. The coordinates of the entry and exit points of the track can also be specified within the device. In 2-D simulations, the track is assumed to be a cylinder with a specified radius. The ehps generated at any point are a function of the radial distance r, from the center of the track to the point, the distance l along the track, and the time, t. ATLAS implements the generation rate as the number of ehps per cm^3 along the track according to the equation

$$G(r,l,t) = x(\text{DENSITY} * L1(l) + S * \text{B.DENSITY} * L2(l)) * R(r) * T(t)$$

where DENSITY and B.DENSITY are defined as the number of generated ehps per cm^{-3}. By setting a PCUNITS parameter, we can specify the charge generated in terms of pC/μm depending on the LET value of the ionizing radiation and the concerned semiconductor as discussed above. The factors $L1$ and $L2$ define the variation in charger or carrier generation along the SEU track. The factor $R(r)$ is the radial parameter and is defined as

$$R(r) = \exp - \frac{r^2}{\text{RADIUS}}. \quad (2)$$

The factor $T(t)$ is the time dependency of the charge generation governed by two user-defined parameters, namely, the temporal Gaussian function width and the initial time of charge generation.

IV. SEE Simulations

The SEEs in Ga_2O_3 MOSFETs are investigated using the single-event upset model in SILVACO TCAD. In accordance with the previous radiation research studies [15], [21], the spatial Gaussian function width is set to 50 nm, the temporal Gaussian function width is set to 2 ps, and the initial time of charge generation is set to 100 ps. The strike location is chosen by studying the electric field profile of the device before radiation. All the simulations for understanding the SEEs are performed in the OFF-state of the MOSFET at a gate bias of V_{gs} =−25 V. As shown in Fig. 3(b), the location in the channel vertically under the edge of the field plate has a very high peak electric field and thus is the most sensitive region for SEEs following an ion strike. Thus, the ion strike path has been chosen as (x, y) = (10,0) to (x, y) = (10,0.4). Thermal simulation models are also included in our simulation for all the cases. The simulation parameters along with the device parameters are shown in Table I.

The MOSFET structure shown in Fig. 1 was simulated under two operating biases and LET = 10 MeV/mg/cm^2 to understand the SEEs. From Fig. 4, it can be seen that there is a peak transient current for both the conditions just after the ion strike, but with time it slowly recovers. However, at V_{ds} = 500 V, a second breakdown mechanism occurs which is discussed below, the current starts to increase and goes beyond the safety limits. Thus, the device recovers under V_{ds} = 220 V but suffers from SEB at V_{ds} = 500 V at

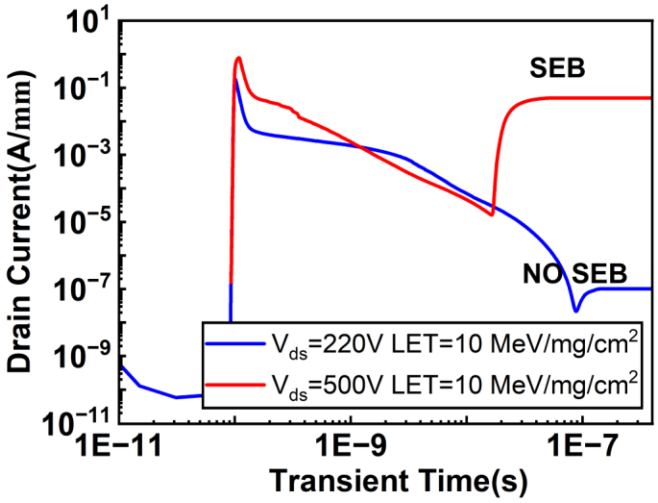

Fig. 4. Transient drain current for the MOSFET at V_{ds} = 220 and 500 V for LET = 10 MeV/mg/cm^2.

TABLE I
DESIGN PARAMETERS IN SIMULATION

Design Parameters	Value
Lgd(Gate to Drain Length)	20 μm
Thickness of dielectric	400 nm
Channel Layer doping	5×17 cm^{-3}
Dielectric constant of SiO2	3.9
Dielectric constant of HfO2	25
Dielectric constant of BaTiO3	100
Spatial Gaussian function width	50 nm [15], [21]
Temporal Gaussian function width	2×10^{-12}s [15], [21]
Initial Time of of charge generation	100e-12 [15], [21]
Length of ion track	10,0 - 10,0.4
Hole recombination time	4×10^{-10}s
Models used	auger, srh, fldmob, impact,lat.temp
Impact Ionization Parameters.	a=0.79×10^6, b=2.92×10^7 [48]

LET = 10 MeV/mg/cm^2. The physics behind the SEB failure can be understood by analyzing the electron–hole concentration profiles and electric field contour at various time instants. Figs. 5 and 6 show the electron and hole concentrations, respectively, in the device at various time instants after the ion strike. At t = 1.04 × 10^{-10} s, which is just after the ion strike, ehps are generated along the ion strike path as shown in Figs. 5(a) and 6(a). Gradually with time, the electrons start to migrate toward the drain and the holes start to migrate toward the gate which is shown in Figs. 5(b) and 6(b). Now as shown in Fig. 7(a), the electric field in the channel is high with peaks under the gate and at the ion strike path. With time as more and more carriers start to accumulate near the gate, the impact generation rate starts to increase gradually. As shown in Fig. 7, initially the impact generation rate was present only under the ion strike path. But with time as more and more holes and electrons started accumulating under the gate, the impact generation rate increased which leads to high electron and hole concentrations in the channel at t = 8 × 10^{-9} onward. At t = 15 × 10^{-9}, the impact generation rate is very high generating a huge concentration of electrons and holes as shown in Figs. 6(d) and 7(d) which are present throughout the channel. This leads to SEB failure with current exceeding the safety limits of 1 mA/mm, [20] as shown in Fig. 4.

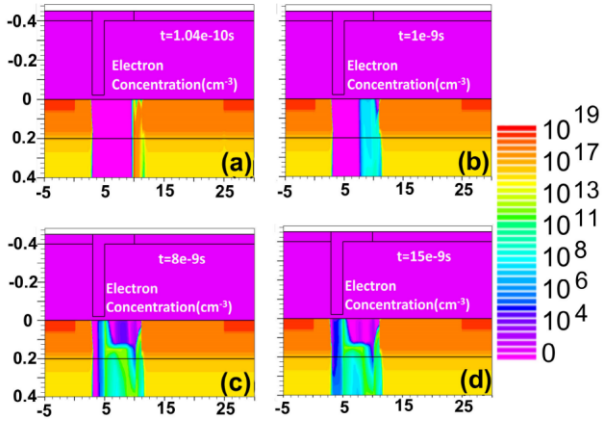

Fig. 5. Electron concentration at various time instants (a) t = 1.04e − 10s, (b) t = 1e −9s, (c) 8e −9s, and (d) t = 15e −9s after the ion strike at V_{ds} = 500 V and LET = 10 MeV/mg/cm^2.

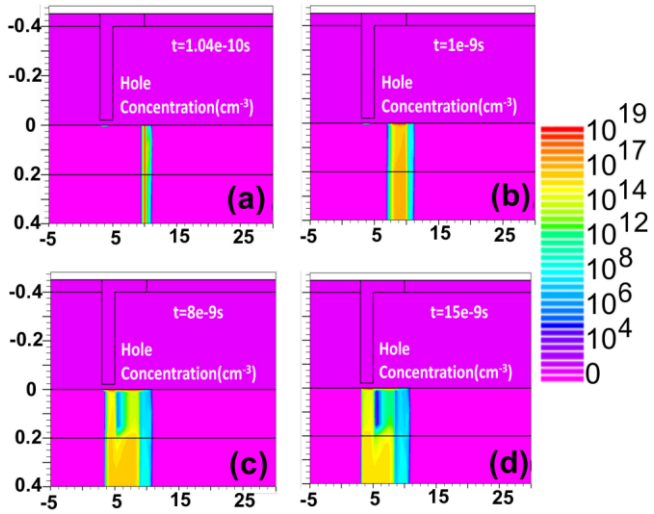

Fig. 6. Hole concentration at various time instants (a) t = 1.04e − 10s, (b) t = 1e − 9s, (c) t = 8e − 9s, and (d) t = 15e − 9s at V_{ds} = 500 V and LET = 10 MeV/mg/cm^2.

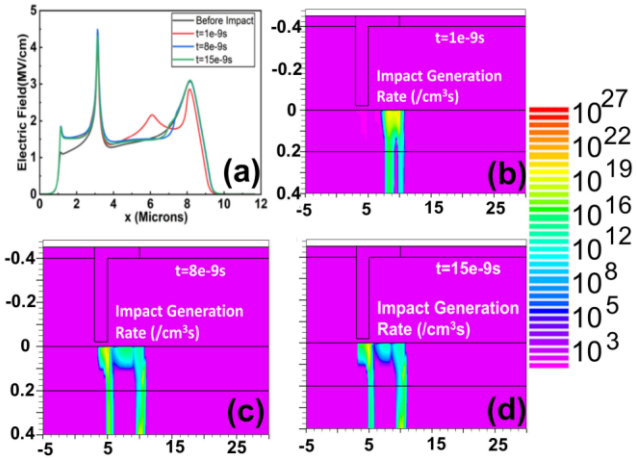

Fig. 7. (a) Electric field profile and impact generation at various time instants, (b) t = 1e − 9s (c) t = 8e − 9s, and (d) t = 15e − 9s at V_{ds} = 500 V and LET = 10 MeV/mg/cm^2.

Thus, with the baseline design the SEB threshold of 220 V at LET = 10 MeV/mg/cm^2 for the Ga_2O_3 MOSFET is lower than the simulated SEB in radiation-hardened GaN HEMTs [20] and AlGaN/GaN-based MISFET [21].

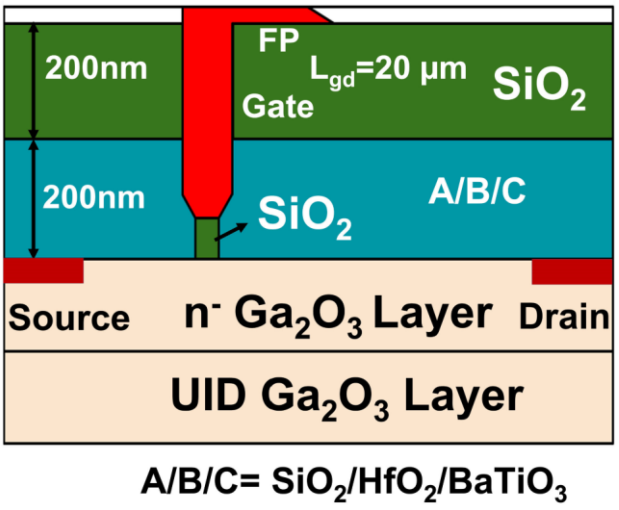

Fig. 8. Schematic of the radiation-hardened MOSFET design.

The mechanism discussed above clearly indicates that the electric field in the channel should be reduced to design radiation-hardened MOSFETs. Thus, a modified design with a high-k dielectric combination is proposed here.

V. Radiation-Hardened Design

As discussed in the earlier section, to reduce the overall electric field in the channel, a MOSFET design with a combination of high-k dielectric and SiO_2 as shown in Fig. 8 is proposed. The first design is proposed with the combination of conventional dielectrics which is HfO_2 and SiO_2. However, due to possible band alignment issues with Ga_2O_3 and HfO_2, the gate dielectric has been kept SiO_2. Gate rounding techniques

have also been implemented to reduce the electric field crowding at the edges and also mimic the simulation as closely as possible to a fabricated structure.

The structure was simulated under two radiation conditions of V_{ds} = 550 V and LET = 10 MeV/mg/cm^2 and V_{ds} = 650 V and LET = 75 MeV/mg/cm^2 At V_{ds} = 550 V and LET = 10 MeV/mg/cm^2, the current recovers, and the leakage current is still within the safe limits indicating that the device has not suffered SEB. To understand how the proposed design helps in increasing the SEB threshold at LET = 10 MeV/mg/cm^2, it is important to look at the electron and hole concentrations and the impact generation rate at various time instants. During the initial period of ion strike, the electrons and holes behave similar to that discussed in the earlier section. There is a peak transient current just after the ion strike as shown in Fig. 9, and then for both the cases, the current starts to recover slowly. However, as shown in Fig. 10(a), the electric field in the channel is lower especially under the gate when compared with the conventional structure though the device is operating at a higher bias. Thus, at $t = 10 \times 10^{-9}$ s, the impact generation rate is significantly lower leading to lower levels of electron and hole concentrations as shown in Fig. 11. As a result, the drain current does increase again. The current stays below the safety limits and SEB is not triggered.

However, for extreme radiation conditions of V_{ds} = 650 V and LET = 75 MeV/mg/cm^2, the device suffers from SEB

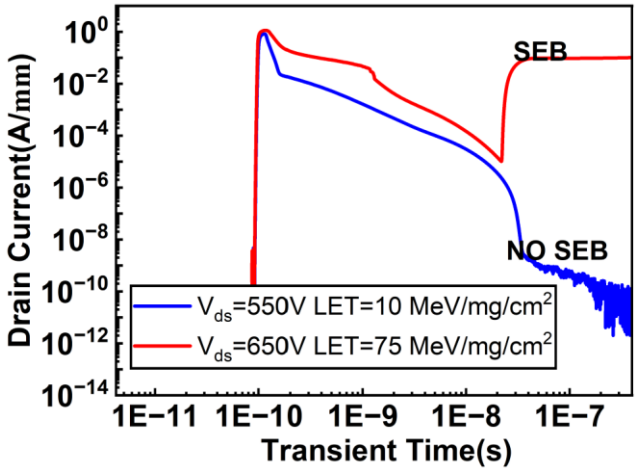

%

Here is how to import EPS art

Fig. 9. Transient drain current for HfO_2–SiO_2 dielectric combination MOSFET for two different radiation conditions.

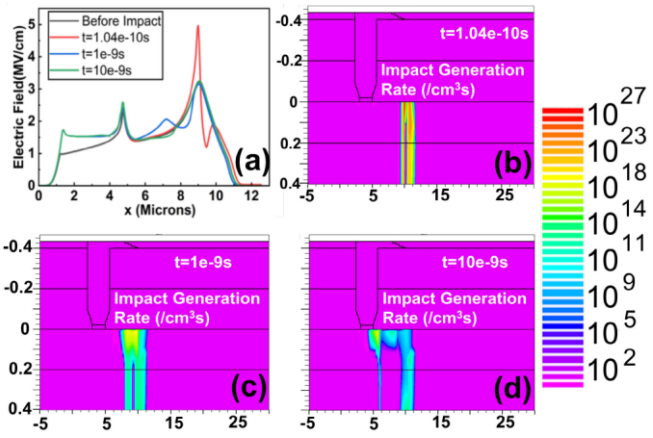

Fig. 10. Electric field and impact generation rate at different time instants for HfO_2–SiO_2 dielectric combination at V_{ds} = 550 V and LET = 10 MeV/mg/cm^2.

because the impact generation rate becomes higher due to higher electric fields in the channel. Thus, to get further radiation hardness, a very high-k dielectric material has to be used.

Here, we have proposed a combination of $BaTiO_3$ and SiO_2 as shown in Fig. 8. Fig. 12 and shows the transient drain current plots under radiation conditions of V_{ds} = 650 V LET = 75 MeV/mg/cm^2 and V_{ds} = 1000 V LET = 75 MeV/mg/cm^2, respectively.

The device shows full current recovery which can be further understood by analyzing the electron, hole, and impact generation rate contour plots at various time instants. As shown in Fig. 13, the electric field is significantly lowered even at a high operating bias of 1000 V, which leads to low impact generation rates in the channel. The electron and hole concentrations are shown from $t = 8 \times 10^{-9}$ s onward since before that the behavior of electrons and holes is similar to the earlier cases. Thus, even though carriers are present in the channel at 8×10^{-9} s, they start to recombine with each other instead of undergoing impact ionization. The result is clearly seen in Fig. 14 where the electron and hole concentrations are very low as time progresses. Therefore, the drain current does

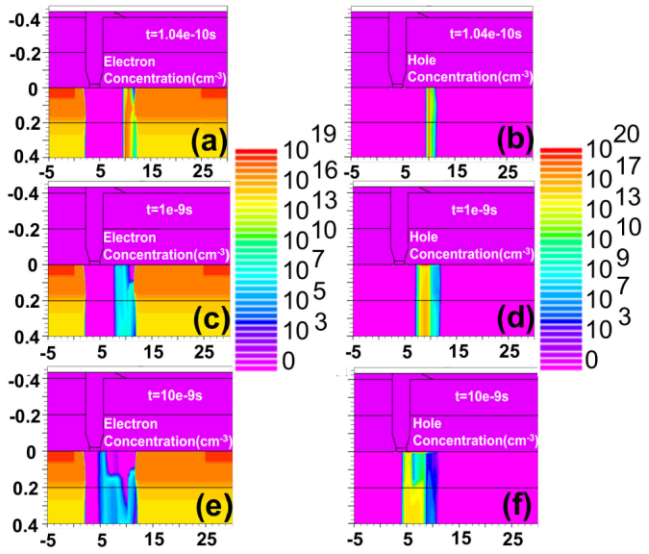

Fig. 11. Electron and hole concentrations at different time instants for HfO_2–SiO_2 dielectric combination at V_{ds} = 550 V and LET = 10 MeV/mg/cm^2.

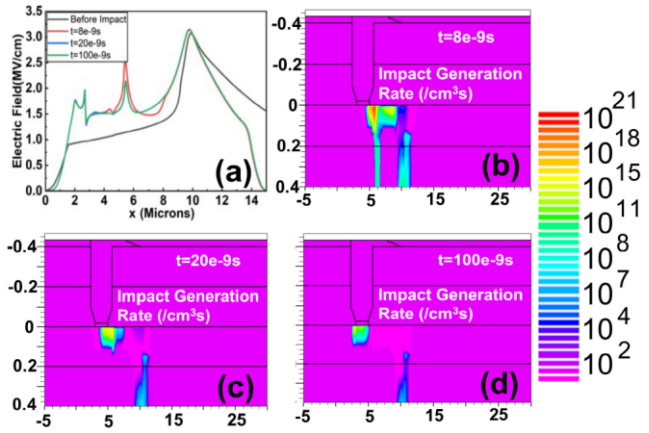

Fig. 13. Electric field profile and impact generation rate for $BaTiO_3$–SiO_2 dielectric combination at various time instants after the ion strike at V_{ds} = 1000 V and LET = 75 MeV/mg/cm^2.

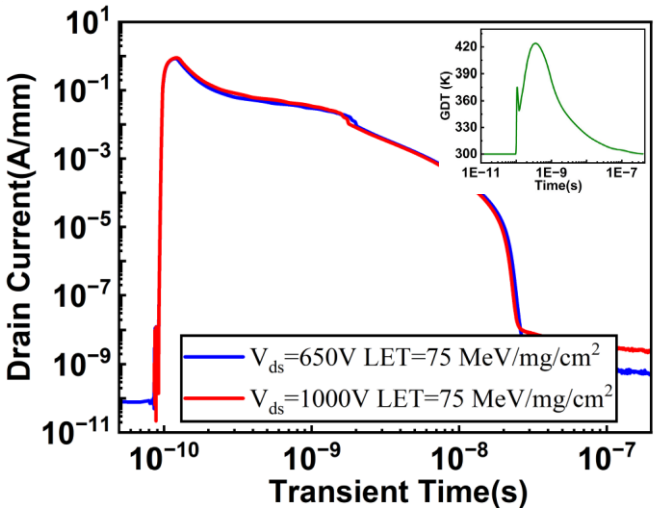

Fig. 12. Transient drain current for $BaTiO_3$–SiO_2 dielectric combination under V_{ds} = 650, 1000 V and LET = 75 MeV/mg/cm^2. The inset shows the variation in GDT with time for V_{ds} = 1000 V and LET = 75 MeV/mg/cm^2.

not increase with time, and the device is immune to extreme radiation conditions.

Ideally, if a high-k dielectric such as HfO_2 or $BaTiO_3$ of higher thickness could be used as a fully dielectric layer for the MOSFET, the radiation hardness could be increased further. However, high leakage currents and challenges of depositing thick dielectrics limit us in using that design.

To further verify our simulations, we have also varied the hole mobility to 2 cm^{2}V^{-1}s^{-1} [54] and have obtained similar results which shows that the hole mobility is not an important factor for determining the SEB threshold condition.

It is noted that thermal simulations were carried out with the ionizing current as heat source for all the conditions described above. The global device temperature (GDT) which is the highest temperature in the device at a time instant did not go beyond 420k (shown in Fig. 12 inset) which is far below

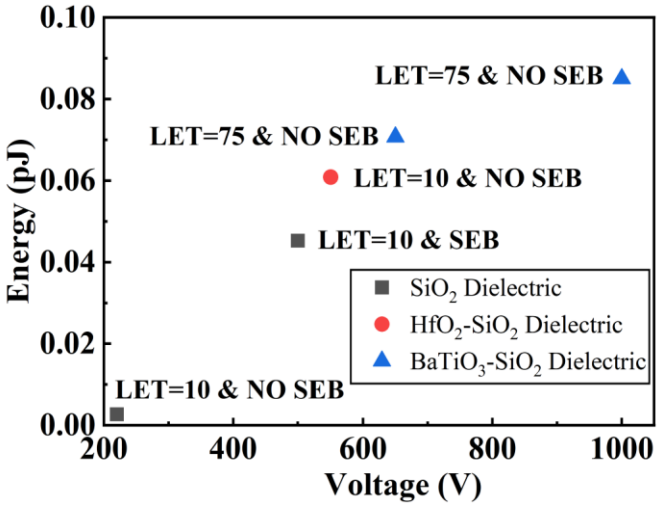

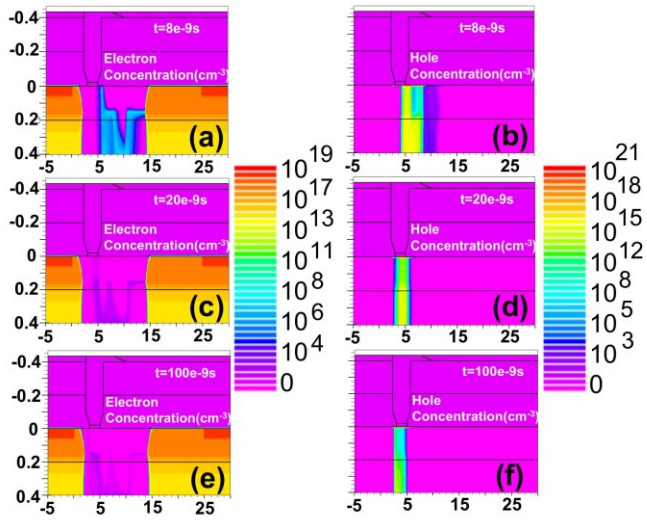

Fig. 14. Electron and hole concentrations for $BaTiO_3$–SiO_2 dielectric combination at various time instants after the ion strike at V_{ds} = 1000 V and LET = 75 MeV/mg/cm^2.

the melting point of Ga_2O_3 and the dielectrics used, ruling out catastrophic thermal failure.

Moreover, we have not investigated the TID effects which could also lead to device reliability issues in harsh radiation environment. The TID effect depends on the dielectric/channel interface. There are reports on TID effects and mitigation techniques in other semiconductor technologies [55], [56]. Similar studies of TID effect needs to be explored in Ga_2O_3 MOSFETs before they can be used in real applications.

VI. Energy Dissipation Calculation

The amount of energy dissipated during the ionizing radiation event in the MOSFET is an important factor in analyzing the radiation hardness of the semiconductor material. The energy dissipated during each event can be calculated by integrating the current density times area of ion track and the electric field along the entire ion track and then integrating temporally. The area of the ion track is taken to be πr^2, where r is the radius of the ion track. The energy dissipated is calculated using the following equation [15]:

$$\text{Energy} \approx \int\int J * A_{\text{ion}} * E_{\text{field}} dx dt. \quad (3)$$

Fig. 15. Energy dissipated during the ion strike event in β-Ga_2O_3 MOSFET for various radiation conditions. LET values are measured in MeV/mg/cm^2.

Fig. 15 shows the energy dissipated for the first 336 ps of the ion strike event in β-Ga_2O_3 MOSFETs under different radiation conditions. It is observed that the power dissipated for ion strike event in Ga_2O_3 MOSFET irrespective of the radiation condition is significantly less than that energy dissipated in SiC MOSFETs [15]. In SiC MOSFETs, as reported an ion strike of LET = 2 MeV/mg/cm^2 at a bias of 1300 V results in energy dissipation of 2.5 nJ, and for LET = 10 MeV/mg/cm^2 at a bias of 500 V, 2.6 nJ of energy is dissipated. This results from the lower ionization rate in Ga_2O_3 due to its large bandgap. The energy dissipated increases with increasing LET and increasing operating bias which is in accordance with our discussion in the earlier sections that with increasing bias and LET, the electric fields could be higher and the transient drain current peaks are higher. However, the energy dissipation factor is not correlated with specific SEB effect as seen in the figure.

VII. Peak Electric Field and SEB Threshold Condition

As discussed in the earlier section, though the energy dissipation in Ga_2O_3 MOSFET is lower than that of SiC MOSFETs, it is not a helpful parameter in determining a specific SEB threshold condition for voltage or LET. The main factor responsible for triggering the SEB mechanism was found to be the electric field. Though our simulations suggest that decreasing the electric field in the channel increases the SEB threshold conditions, it is difficult to identify a specific threshold condition that is applicable for Ga_2O_3 MOSFETs across all the design modifications. Fig. 16 shows the variation in peak electric field in the channel at the location of ion strike at $t = 8 \times 10^{-9}$ s for all the designs. It can be clearly seen that using a high-k dielectric reduces the peak electric fields in the channel but it also changes the overall electric field distribution

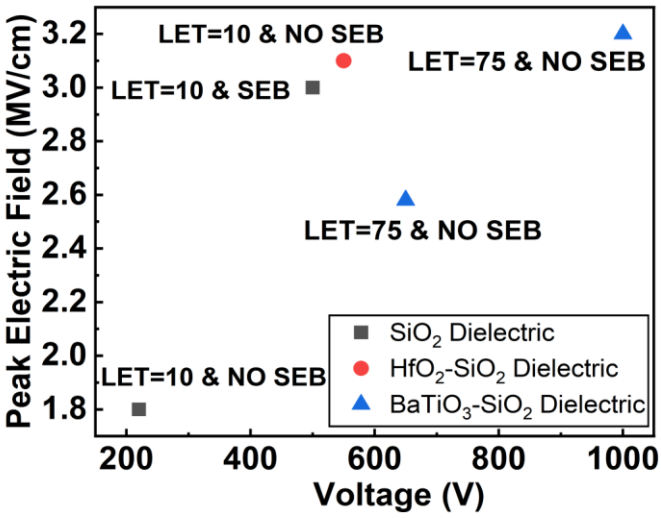

Fig. 16. Peak electric fields in the channel at $t = 8 \times 10^{-9}$ s in the ion strike location for all the designs.

in the device. But the peak electric field value is not the decisive factor for determining the SEB triggering mechanism. The overall electric field distribution affects the total impact generation rate in the device which is responsible for the generation of carriers. For example, if we take radiation condition of V_{ds} = 500 V and LET = 10 MeV/mg/cm^2 for the conventional design shown in Fig. 1 and a radiation condition of V_{ds} = 1000 V and LET = 75 MeV/mg/cm^2 for the modified design shown in Fig. 8 with the $BaTiO_3$ dielectric, the peak electric fields in the channel for the $BaTiO_3$–SiO_2 design are higher as shown in Fig. 16. However, the field distributions are different for the two designs, which leads to different impact generation rates and different levels of electron and hole concentrations as discussed earlier. Thus, even though the peak electric field value is higher the $BaTiO_3$–SiO_2 design combination does not suffer from SEB, whereas in the SiO_2 design, SEB is triggered.

VIII. Conclusion

In this article, detailed 2-D TCAD simulations were performed to investigate the SEEs in β-Ga_2O_3 MOSFETs. The physics behind the SEB mechanism is understood and the electric field distribution in the channel is one of the main factors behind the SEB triggering mechanism. Our initial simulations suggest that the SEB threshold voltage of the baseline lateral Ga_2O_3 MOSFET is lower than the simulated SEB threshold in the state-of-the-art AlGaN/GaN HEMTs and MISFETs. Thus keeping in mind the physics behind the SEB

mechanism, radiation hardening techniques are proposed which show improved radiation-hardened performance. To reduce the high electric fields in the channel responsible for the high impact generation rates, a radiation-hardened device with rounded gates and high-*k* dielectric was proposed. The high-*k* dielectric is used in combination with SiO_2 to reduce the fabrication challenges associated with depositing a thick layer of high*k* dielectric. First, with HfO_2–SiO_2 dielectric combination, an SEB threshold voltage of 550 V is obtained which is higher than that of GaN HEMTs. However, this design also fails under extreme radiation conditions. Therefore, it is proposed that to operate under extreme radiation conditions, a very high*k* dielectric material such as $BaTiO_3$ could be used which reduces the overall electric field distribution in the channel significantly. With this design, the device can achieve SEB thresholds going up to 1000 V at LET = 75 MeV/mg/cm^2. Another technique that could be explored to design radiationhardened β-Ga_2O_3 MOSFETs is using a p-type material such as p-NiO, which is also helpful in reducing the electric field in the channel. Though the energy dissipation is not correlated with the SEB threshold, our calculations show that energy dissipation during SEB strike in Ga_2O_3 MOSFETs is lower than that in SiC MOSFETs.

References

[1] J. R. Srour and J. W. Palko, "A framework for understanding displacement damage mechanisms in irradiated silicon devices," *IEEE Trans. Nucl. Sci.*, vol. 53, no. 6, pp. 3610–3620, Dec. 2006, doi: 10.1109/TNS.2006.885796.

[2] N. A. Dodds et al., "The contribution of low-energy protons to the total on-orbit SEU rate," *IEEE Trans. Nucl. Sci.*, vol. 62, no. 6, pp. 2440–2451, Dec. 2015, doi: 10.1109/TNS.2015.2486763.

[3] M. J. Martinez et al., "Radiation response of AlGaN-channel HEMTs," *IEEE Trans. Nucl. Sci.*, vol. 66, no. 1, pp. 344–351, Jan. 2019, doi: 10.1109/TNS.2018.2885526.

[4] J. Kim et al., "Radiation damage effects in Ga_2O_3 materials and devices," *J. Mater. Chem. C*, vol. 7, no. 1, pp. 10–24, 2019, doi: 10.1039/C8TC04193H.

[5] D. C. Look, D. C. Reynolds, J. W. Hemsky, J. R. Sizelove, R. L. Jones, and R. J. Molnar, "Defect donor and acceptor in GaN," *Phys. Rev. Lett.*, vol. 79, no. 12, pp. 2273–2276, Sep. 1997, doi: 10.1103/PhysRevLett.79.2273.

[6] A. Ionascut-Nedelcescu, C. Carlone, A. Houdayer, H. J. von Bardeleben, J.-L. Cantin, and S. Raymond, "Radiation hardness of gallium nitride," *IEEE Trans. Nucl. Sci.*, vol. 49, no. 6, pp. 2733–2738, Dec. 2002, doi: 10.1109/TNS.2002.805363.

[7] A. L. Barry, B. Lehmann, D. Fritsch, and D. Braunig, "Energy dependence of electron damage and displacement threshold energy in 6H silicon carbide," *IEEE Trans. Nucl. Sci.*, vol. 38, no. 6, pp. 1111–1115, Dec. 1991, doi: 10.1109/23.124082.

[8] A. F. Witulski et al., "Single-event burnout of SiC junction barrier Schottky diode high-voltage power devices," *IEEE Trans. Nucl. Sci.*, vol. 65, no. 1, pp. 256–261, Jan. 2018, doi: 10.1109/TNS.2017.2782227. [9] M.-B. Li, F. Cao, H.-F. Hu, X.-J. Li, J.-Q. Yang, and Y. Wang, "High single-event burnout resistance 4H-SiC junction barrier Schottky diode," *IEEE J. Electron Devices Soc.*, vol. 9, pp. 591–598, May 2021, doi: 10.1109/JEDS.2021.3084797.

[10] J. A. McPherson, P. J. Kowal, G. K. Pandey, T. P. Chow, W. Ji, and A. A. Woodworth, "Heavy ion transport modeling for single-event burnout in SiC-based power devices," *IEEE Trans. Nucl. Sci.*, vol. 66, no. 1, pp. 474–481, Jan. 2019, doi: 10.1109/TNS.2018.2880865.

[11] A. Javanainen et al., "Heavy ion induced degradation in SiC Schottky diodes: Bias and energy deposition dependence," *IEEE Trans. Nucl. Sci.*, vol. 64, no. 1, pp. 415–420, Jan. 2017, doi: 10.1109/TNS.2016.2616921.

[12] E. Mizuta, S. Kuboyama, H. Abe, Y. Iwata, and T. Tamura, "Investigation of single-event damages on silicon carbide (SiC) power MOSFETs," *IEEE Trans. Nucl. Sci.*, vol. 61, no. 4, pp. 1924–1928, Aug. 2014, doi: 10.1109/TNS.2014.2336911.

[13] T. Makino et al., "Heavy-ion induced anomalous charge collection from 4H-SiC Schottky barrier diodes," *IEEE Trans. Nucl. Sci.*, vol. 60, no. 4, pp. 2647–2650, Aug. 2013, doi: 10.1109/TNS.2013.2243469.

[14] S. Kuboyama, C. Kamezawa, N. Ikeda, T. Hirao, and H. Ohyama, "Anomalous charge collection in silicon carbide Schottky barrier diodes and resulting permanent damage and single-event burnout," *IEEE Trans. Nucl. Sci.*, vol. 53, no. 6, pp. 3343–3348, Dec. 2006, doi: 10.1109/TNS.2006.885165.

[15] D. R. Ball et al., "Ion-induced energy pulse mechanism for singleevent burnout in high-voltage SiC power MOSFETs and junction barrier Schottky diodes," *IEEE Trans. Nucl. Sci.*, vol. 67, no. 1, pp. 22–28, Jan. 2020, doi: 10.1109/TNS.2019.2955922.

[16] S. J. Pearton, Y.-S. Hwang, and F. Ren, "Radiation effects in GaN-based high electron mobility transistors," *JOM*, vol. 67, no. 7, pp. 1601–1611, Mar. 2015, doi: 10.1007/s11837-015-1359-y.

[17] I.-H. Lee et al., "Defects responsible for lifetime degradation in electron irradiated n-GaN grown by hydride vapor phase epitaxy," *Appl. Phys. Lett.*, vol. 110, no. 11, Mar. 2017, Art. no. 112102, doi: 10.1063/1.4978641.

[18] A. Yadav et al., "Low and moderate dose gamma-irradiation and annealing impact on electronic and electrical properties of AlGaN/GaN high electron mobility transistors," *Radiat. Effects Defects Solids*, vol. 170, no. 5, pp. 377–385, Mar. 2015, doi: 10.1080/10420150.2015.1010170.

[19] E. E. Patrick, M. Choudhury, F. Ren, S. J. Pearton, and M. E. Law, "Simulation of radiation effects in AlGaN/GaN HEMTs," *ECS J. Solid State Sci. Technol.*, vol. 4, no. 3, pp. 21–25, Jan. 2015, doi: 10.1149/2.0181503jss.

[20] S. Liu et al., "Simulation research on single event burnout performances of p-GaN gate HEMTs with 2DEG $Al_xGa_{1-x}N$ channel," *IEEE Trans. Electron Devices*, vol. 69, no. 3, pp. 973–980, Mar. 2022, doi: 10.1109/TED.2022.3141985.

[21] X. Luo et al., "Research of single-event burnout and hardening of AlGaN/GaN-based MISFET," *IEEE Trans. Electron Devices*, vol. 66, no. 2, pp. 1118–1122, Feb. 2019, doi: 10.1109/TED.2018.2887245.

[22] J. Y. Tsao et al., "Ultrawide-bandgap semiconductors: Research opportunities and challenges," *Adv. Electron. Mater.*, vol. 4, no. 1, Dec. 2018, Art. no. 1600501, doi: 10.1002/aelm.201600501.

[23] M. J. Tadjer et al., "Structural, optical, and electrical characterization of monoclinic β-Ga_2O_3 grown by MOVPE on sapphire substrates," *J. Electron. Mater.*, vol. 45, no. 4, pp. 2031–2037, Feb. 2016, doi: 10.1007/s11664-016-4346-3.

[24] M. Baldini, M. Albrecht, A. Fiedler, K. Irmscher, R. Schewski, and G. Wagner, "Editors' choice—Si- and sn-doped homoepitaxial β-Ga_2O_3 layers grown by MOVPE on (010)-oriented substrates," *ECS J. Solid State Sci. Technol.*, vol. 6, no. 2, pp. 3040–3044, Oct. 2016, doi: 10.1149/2.0081702jss.

[25] Z. Galazka et al., "Scaling-up of bulk β-Ga_2O_3 single crystals by the Czochralski method," *ECS J. Solid State Sci. Technol.*, vol. 6, no. 2, pp. 3007–3011, Sep. 2016, doi: 10.1149/2.0021702jss.

[26] S. Stepanov, V. Nikolaev, V. Bougrov, and A. Romanov, "Gallium oxide: Properties and applica 498 a review," *Rev. Adv. Mater. Sci*, vol. 44, pp. 63–86, Nov. 2016.

[27] A. Bhattacharyya et al., "Multi-kV class β-Ga_2O_3 MESFETs with a lateral figure of merit up to 355 MW/cm^2," *IEEE Electron Device Lett.*, vol. 42, no. 9, pp. 1272–1275, Sep. 2021, doi: 10.1109/LED.2021.3100802.

[28] A. Bhattacharyya et al., "4.4 kV β-Ga_2O_3 MESFETs with power figure of merit exceeding 100 MW cm^2," *Appl. Phys. Exp.*, vol. 15, no. 6, May 2022, Art. no. 061001, doi: 10.35848/1882-0786/ ac6729.

[29] S. Sharma, K. Zeng, S. Saha, and U. Singisetti, "Field-plated lateral Ga_2O_3 MOSFETs with polymer passivation and 8.03 kV breakdown voltage," *IEEE*

Electron Device Lett., vol. 41, no. 6, pp. 836–839, Jun. 2020, doi: 10.1109/LED.2020.2991146.

[30] K. Zeng, A. Vaidya, and U. Singisetti, "A field-plated Ga_2O_3 MOSFET with near 2-kV breakdown voltage and 520 m$\Omega \cdot cm^2$ on-resistance," *Appl. Phys. Exp.*, vol. 12, no. 8, Jul. 2019, Art. no. 081003, doi: 10.7567/1882-0786/ab2e86.

[31] J. K. Mun, K. Cho, W. Chang, H.-W. Jung, and J. Do, "2.32 kV breakdown voltage lateral β-Ga_2O_3 MOSFETs with source-connected field plate," *ECS J. Solid State Sci. Technol.*, vol. 8, no. 7, pp. 3079–3082, Feb. 2019, doi: 10.1149/2.0151907jss.

[32] K. D. Chabak et al., "Enhancement-mode Ga_2O_3 wrap-gate fin field-effect transistors on native (100) β-Ga_2O_3 substrate with high breakdown voltage," *Appl. Phys. Lett.*, vol. 109, no. 21, Nov. 2016, Art. no. 213501, doi: 10.1063/1.4967931.

[33] Y. Lv et al., "Lateral β-Ga_2O_3 MOSFETs with high power figure of merit of 277 MW/cm^2," *IEEE Electron Device Lett.*, vol. 41, no. 4, pp. 537–540, Apr. 2020, doi: 10.1109/LED.2020. 2974515.

[34] W. Li et al., "1.5 kV vertical Ga_2O_3 trench-MIS Schottky barrier diodes," in *Proc. 76th Device Res. Conf. (DRC)*, Jun. 2018, pp. 1–2, doi: 10.1109/DRC.2018.8442245.

[35] M. Higashiwaki and S. Fujita, *Gallium Oxide: Materials Properties, Crystal Growth, and Devices*, vol. 293. Berlin, Germany: Springer, 2020.

[36] J. Zhang et al., "Ultra-wide bandgap semiconductor Ga_2O_3 power diodes," *Nature Commun.*, vol. 13, no. 1, pp. 1–8, Jul. 2022, doi: 10.1038/s41467-022-31664-y.

[37] S. Roy, A. Bhattacharyya, C. Peterson, and S. Krishnamoorthy, "β-Ga_2O_3 lateral high-permittivity dielectric superjunction Schottky barrier diode with 1.34 GW/cm^2 power figure of merit," *IEEE Electron Device Lett.*, vol. 43, no. 12, pp. 2037–2040, Dec. 2022, doi: 10.1109/LED.2022.3216302.

[38] S. Roy, A. Bhattacharyya, P. Ranga, H. Splawn, J. Leach, and S. Krishnamoorthy, "High-k oxide field-plated vertical (001) β-Ga_2O_3 Schottky barrier diode with Baliga's figure of merit over 1 GW/cm^2," *IEEE Electron Device Lett.*, vol. 42, no. 8, pp. 1140–1143, Aug. 2021, doi: 10.1109/LED.2021.3089945.

[39] M. H. Wong et al., "Radiation hardness of β-Ga_2O_3 metal-oxidesemiconductor field-effect transistors against gamma-ray irradiation," *Appl. Phys. Lett.*, vol. 112, no. 2, Jan. 2018, Art. no. 023503, doi: 10.1063/1.5017810.

[40] R. Lingaparthi et al., "Surface related tunneling leakage in β-Ga_2O_3 (001) vertical Schottky barrier diodes," *Appl. Phys. Exp.*, vol. 12, no. 7, Jun. 2019, Art. no. 074008, doi: 10.7567/1882-0786/ab2824.

[41] A. Y. Polyakov, V. I. Nikolaev, E. B. Yakimov, F. Ren, S. J. Pearton, and J. Kim, "Deep level defect states in β-, α-, and ϵ-Ga_2O_3 crystals and films: Impact on device performance," *J. Vac. Sci. Technol. A*, vol. 40, no. 2, Feb. 2022, Art. no. 020804, doi: 10.1116/6.0001701.

[42] E. B. Yakimov et al., "Experimental estimation of electron-hole pair creation energy in β-Ga_2O_3," *Appl. Phys. Lett.*, vol. 118, no. 20, May 2021, Art. no. 202106, doi: 10.1063/5.0053301.

[43] Z. Xia et al., "Metal/$BaTiO_3$/β-Ga_2O_3 dielectric heterojunction diode with 5.7 MV/cm breakdown field," *Appl. Phys. Lett.*, vol. 115, no. 25, Dec. 2019, Art. no. 252104, doi: 10.1063/1.5130669.

[44] T. Razzak et al., "$BaTiO_3$/$Al_{0.58}Ga_{0.42}N$ lateral heterojunction diodes with breakdown field exceeding 8 MV/cm," *Appl. Phys. Lett.*, vol. 116, no. 2, Jan. 2020, Art. no. 023507, doi: 10.1063/1.5130590.

[45] M. W. Rahman, N. K. Kalarickal, H. Lee, T. Razzak, and S. Rajan, "Integration of high permittivity $BaTiO_3$ with AlGaN/GaN for neartheoretical breakdown field kV-class transistors," *Appl. Phys. Lett.*, vol. 119, no. 19, Nov. 2021, Art. no. 193501, doi: 10.1063/5.0070665.

[46] K. Ghosh and U. Singisetti, "Ab initio calculation of electron–phonon coupling in monoclinic β-Ga_2O_3 crystal," *Appl. Phys. Lett.*, vol. 109, no. 7, Aug. 2016, Art. no. 072102, doi: 10.1063/1.4961308.

[47] K. Ghosh and U. Singisetti, "Electron mobility in monoclinic βGa_2O_3—Effect of plasmon-phonon coupling, anisotropy, and confinement," *J. Mater. Res.*, vol. 32, no. 22, pp. 4142–4152, Oct. 2017, doi: 10.1557/jmr.2017.398.

[48] K. Ghosh and U. Singisetti, "Impact ionization in β-Ga_2O_3," *J. Appl. Phys.*, vol. 124, no. 8, Aug. 2018, Art. no. 085707, doi: 10.1063/1.5034120.

[49] T. Usui, C. A. Donnelly, M. Logar, R. Sinclair, J. Schoonman, and F. B. Prinz, "Approaching the limits of dielectric breakdown for SiO_2 films deposited by plasma-enhanced atomic layer deposition," *Acta Mater.*, vol. 61, no. 20, pp. 7660–7670, Dec. 2013, doi: 10.1016/j.actamat.2013.09.003.

[50] A. F. Witulski et al., "Single-event burnout mechanisms in SiC power MOSFETs," *IEEE Trans. Nucl. Sci.*, vol. 65, no. 8, pp. 1951–1955, Aug. 2018, doi: 10.1109/TNS.2018.2849405.

[51] A. Khachatrian et al., "Application of a focused, pulsed X-ray beam to the investigation of single-event transients in $Al_{0.3}Ga_{0.7}N$/GaN HEMTs," *IEEE Trans. Nucl. Sci.*, vol. 64, no. 1, pp. 97–105, Jan. 2017, doi: 10.1109/TNS.2016.2641678.

[52] R. C. Alig and S. Bloom, "Electron-hole-pair creation energies in semiconductors," *Phys. Rev. Lett.*, vol. 35, no. 22, pp. 1522–1525, Dec. 1975, doi: 10.1103/PhysRevLett.35.1522.

[53] T. R. Weatherford, "Radiation effects in high speed III-V integrated circuits," *Int. J. High Speed Electron. Syst.*, vol. 13, no. 01, pp. 277–292, Mar. 2003, doi: 10.1142/S0129156403001612.

[54] C. Ma et al., "Exploring the feasibility and conduction mechanisms of P-type nitrogen-doped β-Ga_2O_3 with high hole mobility," *J. Mater. Chem. C*, vol. 10, no. 17, pp. 6673–6681, May 2022, doi: 10.1039/D1TC05324H.

[55] C. Chong, H. Liu, S. Wang, and X. Wu, "Research on total ionizing dose effect and reinforcement of SOI-TFET," *Micromachines*, vol. 12, no. 10, p. 1232, Oct. 2021, doi: 10.3390/mi12101232.

[56] S.-H. Hwang, K. Yatsu, D.-H. Lee, I.-J. Park, and H.-I. Kwon, "Effects of Al_2O_3 surface passivation on the radiation hardness of IGTO thin films for thin-film transistor applications," *Appl. Surf. Sci.*, vol. 578, Mar. 2022, Art. no. 152096, doi: 10.1016/j.apsusc.2021.152096.